

EurJIC

European Journal of Inorganic Chemistry

 **Chemistry
Europe**

European Chemical
Societies Publishing

Accepted Article

Title: Spin crossover vs. high-spin iron(II) complexes in N₄S₂ coordination sphere containing picolyl-thioether ligands and NCE (E = S, Se and BH₃) co-ligands

Authors: Diego Plaza-Lozano, Agustín Conde-Gallardo, and Juan Olguin

This manuscript has been accepted after peer review and appears as an Accepted Article online prior to editing, proofing, and formal publication of the final Version of Record (VoR). This work is currently citable by using the Digital Object Identifier (DOI) given below. The VoR will be published online in Early View as soon as possible and may be different to this Accepted Article as a result of editing. Readers should obtain the VoR from the journal website shown below when it is published to ensure accuracy of information. The authors are responsible for the content of this Accepted Article.

To be cited as: *Eur. J. Inorg. Chem.* 10.1002/ejic.202100355

Link to VoR: <https://doi.org/10.1002/ejic.202100355>

WILEY-VCH

Spin crossover vs. high-spin iron(II) complexes in N_4S_2 coordination sphere containing picolyl-thioether ligands and NCE (E = S, Se and BH_3) co-ligands

Diego Plaza-Lozano^[a], Agustín Conde-Gallardo^[b] and Juan Olguín^{*[a]}

[a] D. Plaza-Lozano and Dr. J. Olguín
Departamento de Química
Centro de Investigación y de Estudios Avanzados del IPN (Cinvestav)
Avenida IPN 2508, Col. San Pedro Zacatenco, Ciudad de México 07360, México
E-mail: jolquin@cinvestav.mx

[b] Dr. A. Conde-Gallardo
Departamento de Física
Centro de Investigación y de Estudios Avanzados del IPN (Cinvestav)
Avenida IPN 2508, Col. San Pedro Zacatenco, Ciudad de México 07360, México

Supporting information for this article is given via a link at the end of the document.

Abstract: To study the effect of the chelate ring size on the magnetic properties of thioether-based iron(II) metal complexes, two ligands have been envisaged, synthesised and characterised. The two ligands correspond to the bidentate benzylpicolylthioether (**PySBn**) and tetradentate 2,3-bis(((2-pyridylmethyl)thio)methyl)quinoxaline (**QuinoxS**). Five iron(II) complexes have been synthesised, containing either two bidentate ligands or one tetradentate ligand, and two N-bond NCE co-ligands (E = S, Se or BH_3): *trans*-[Fe^{II}(PySBn)₂(NCE)₂] (**1a-b**) and *cis*-[Fe^{II}(QuinoxS)(NCE)₂] (**2a-c**), **a** for E = S, **b** for E = Se and **c** for E = BH_3 . The iron(II) complexes have been characterised by standard techniques, X-ray crystallography (except for complex **1a**) and VT-magnetic measurements in the solid state. X-ray crystallography showed that all the complexes are isolated in the high spin (HS) state, based on the relatively long Fe-L bond lengths, Fe-N > 2.0 Å and Fe-S ≈ 2.5-2.6 Å. VT-magnetic measurements demonstrated that complexes **1a** and **2a-c** are stabilised in the HS-state, showing orbital contribution to *g* and zero field splitting. However, complex **1b** shows a relatively abrupt, hysteretic, and incomplete at the low-end spin conversion, with $T_{1/2\downarrow} = 92$, $T_{1/2\uparrow} = 98$ K and $\Delta T_{1/2} = 6$ K at 5 K min⁻¹, moreover, the hysteresis loop is scan rate dependent increasing up to 11 K at 10 K min⁻¹. An analysis of structural and electronic parameters has been performed to rationalise the differing magnetic properties of the metal complexes, such as metallacycle size, bond lengths and angles, and *cis*- vs. *trans*-coordination mode. A comparison with the literature-reported spin crossover iron(II) complexes in N_4S_2 coordination sphere containing NCE co-ligands has been conducted as well, finding that, as previously reported, the Fe-N-C(E) bond angle is diagnostic for determining the spin lability of the metal complexes, and in addition we have found that the N—C(E) bond length is too useful.

Introduction

The spin crossover (SCO) effect, that is the reversible interconversion between the low- and high-spin state (LS and HS, respectively) by means of an external stimulus (e.g., temperature, light, magnetic field, solvation/desolvation), can be observed in some first row transition metal complexes

possessing d^4 to d^7 electronic configurations, mostly in octahedral geometries.^[1–3] Due to the differences in the physicochemical properties of the HS and LS-states, this type of materials can be used as molecular switches and sensors,^[4–6] and when the spin transition is accompanied by hysteresis these materials could be used as nanodevices for information storage.^[5,7–12]

The most widely studied SCO system is iron(II) complexes where the metal centre is surrounded by six nitrogen donors, however there are fewer examples of other metal centres and geometries.^[13–16] In addition to the N_6 coordination sphere, recently, it has been demonstrated that N_4S_2 systems can produce iron(II) SCO-active complexes, with only a handful of ligands that can provide the right ligand field for SCO to occur.^[17–23] Figure 1. All the S-based ligands contain the same thioether functional group, in combination with amine, pyridine, triazole or pyrazole nitrogen donors, and some of them contain NCE (E = S, Se or BH_3) co-ligands. An advantage of synthesizing S-containing iron(II) complexes is the protection toward oxidation of the metal centre, as it has been shown that some S-based ligands are redox non-innocent,^[24–27] preventing the metal centre to oxidize to iron(III), thus ensuring the preservation of the SCO-properties.

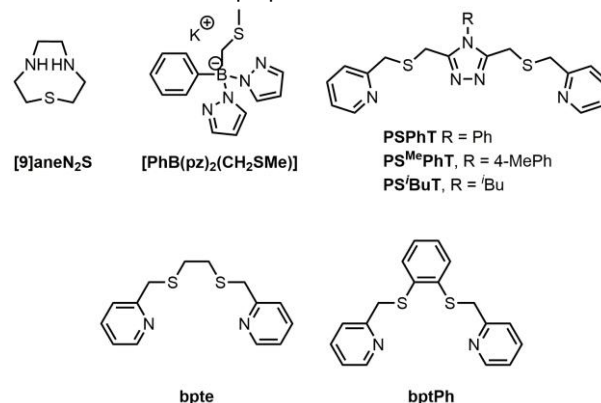


Figure 1. All seven ligands feature thioether donors capable to provide SCO-active Fe^{II} complexes.

To expand the number and type of ligands that can produce SCO-active iron(II) complexes we have synthesised two ligands containing pyridyl and thioether moieties, Figure 2, inspired by the **bpte**^[22] and **bptPh**^[23] ligands (Figure 1). The first ligand is the bidentate picolylthioether (**PySBn**), to evaluate if such a simple ligand can produce SCO active complexes as it contains both S and N donors, and upon coordination to iron(II), five-membered chelate rings are exclusively formed (Figure 2), as well as in the literature reported complexes of **bpte** and **bptPh** ligands. The second ligand is the tetradentate 2,3-bis((2-pyridylmethyl)thio)methyl)quinoxaline (**QuinoxS**), that structurally resembles to **bptPh**, however, the phenyl ring has been replaced by a quinoxaline heterocycle, and an extra methylene group has been incorporated in between the aromatic and sulphur groups, thus the resulting metal complex will contain a seven-membered chelate ring, Figure 2, instead of a five-membered ring as in the **bptPh**-based complex. In addition, the fused heterocycle quinoxaline in **QuinoxS** could promote π - π interactions, and H-bonds due to the spare sp^2 nitrogen atoms, such supramolecular interactions are desired to be present in iron(II) complexes to promote cooperativity in the system, increasing the odds of obtaining SCO systems.

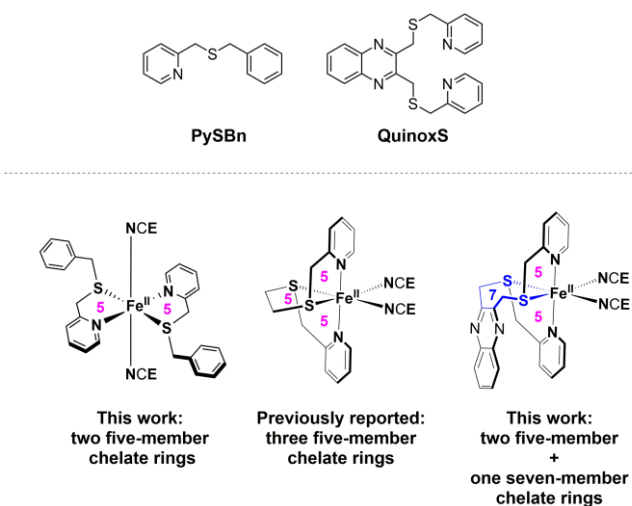


Figure 2. Top: structure of the ligands used in this work. Bottom: structure of the complexes synthesised in this work and the literature reported SCO-active complex, highlighting the chelate ring size.

A series of five metal complexes of the type $[\text{Fe}^{\text{II}}(\text{L})_n(\text{NCE})_2]$, $n = 1$ and $E = \text{S}, \text{Se}$ or BH_3 , for **QuinoxS**, whereas $n = 2$ and $E = \text{S}$ or Se , for **PySBn**, have been synthesised and characterised by standard methods and magnetometry. In addition, single crystal X-ray crystallography has been used for the characterisation of most of the complexes. The use of NCE anions is very common to produce SCO-complexes, since the crystal field can be increased in the order $\text{S} < \text{Se} < \text{BH}_3$.^[28] Thus, two types of metal complexes in N_4S_2 octahedral geometry have been successfully obtained and magnetically characterised. One class of complexes contain the metal centre surrounded by two bidentate ligands, where each ligand strand encompasses a pyridyl unit as N-donor, and a thioether group as S-donor. The second type contains one tetradentate ligand strand, comprising picolylthioether pendant arms. For both types of complexes two NCE co-ligands complete the octahedral coordination sphere,

but in the case of **QuinoxS**-based complexes they are found in a *cis*-arrangement, whereas in the **PySBn**-complexes are found in a *trans*-manner. The effect of chelate ring size on the magnetic properties of the complexes synthesised in this work and the SCO-active complexes reported in the literature has been evaluated (Figure 2), and an analysis of the structural factors affecting the magnetic properties, such as Fe–L bond lengths and angles is presented as well.

Results and Discussion

Synthesis of the ligands

The **PySBn** ligand was synthesised according to the published method with slight modifications,^[29] Figure 3, by reacting an equimolar mixture of benzyl chloride, sodium hydroxide and picolylthiol^[30] in refluxing ethanol. The ligand **PySBn** was obtained in a 91 % yield as a red oil, which crystallised at 0–5 °C, and it was used without further purification. The ligand **QuinoxS** was synthesised according to the procedure reported in the literature,^[31] Figure 3, as a dark beige solid in 86 % yield. All the ligands were characterised by ¹H- and ¹³C{¹H}-NMR, IR and mass spectrometry, confirming the proposed structures, see supporting information.

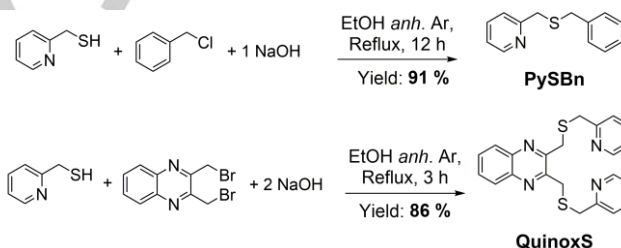


Figure 3. Synthetic procedure for the obtention of **PySBn** and **QuinoxS** ligands.

Synthesis of the metal complexes

The family of complexes **1** were obtained by reaction of one equivalent of *in situ* synthesised $[\text{Fe}^{\text{II}}(\text{Solv.})_4(\text{NCE})_2]$ ($E = \text{S}$ or Se), with two equivalents of **PySBn**, in an adequate solvent under Ar, Figure 4. It is important to mention that the synthesis of the $E = \text{BH}_3$ analogue for **PySBn** was attempted, however it was not possible to obtain a clean sample, and due to COVID-19 pandemic, we have not been able to access research facilities in Mexico since the begging of the health emergency. Whereas, the family of complexes **2** was obtained by treatment of the corresponding *trans*- $[\text{Fe}^{\text{II}}(\text{Py})_4(\text{NCE})_2]$ ^[32] ($E = \text{S}, \text{Se}$ or BH_3) complex with one equivalent of **QuinoxS** ligand, in an adequate solvent under Ar, Figure 4.

To obtain crystals suitable for X-ray crystallography, in most cases, the complexes were obtained by slow diffusion of a solution of the precursor metal complex layered over a solution of the ligand in an adequate solvent (see experimental section), after slow diffusion, crystals suitable for X-ray diffraction were obtained in moderate or good yield, Table 1. However, in the case of **1b** the filtered reaction solution was subjected to diethyl ether vapor diffusion in air at room temperature, and after 24–48 h crystals suitable for X-ray crystallography were obtained.

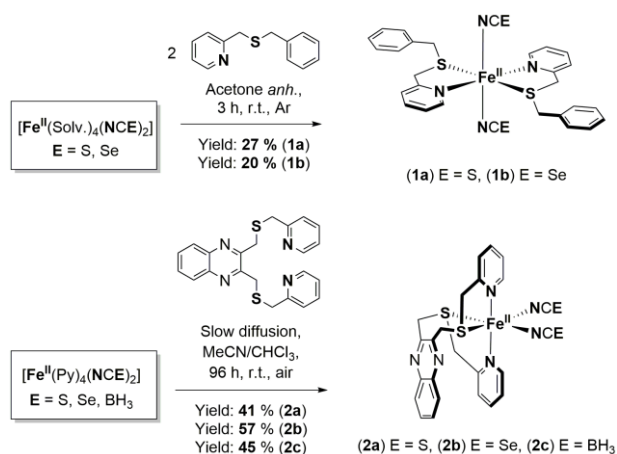


Figure 4. Synthetic methodologies for the obtention of complex families 1 and 2.

Table 1. Crystallisation method, yield, and relevant IR parameters for complex families 1 and 2.

Complex	Crystallisation method	Yield (%)	ν NCE ^[a] (cm ⁻¹)	ν B-H (cm ⁻¹)
1a	-	27 (80) ^[a]	2059	-
1b	Et ₂ O vapor diffusion	20 (15) ^[a]	2059	-
2a	Slow diffusion	41	2070, 2053	-
2b	Slow diffusion	57	2061, 2040	-
2c	Slow diffusion	45	2179	2349, 2321

[a] Yields in parenthesis were obtained from the reaction using precursor complex $\text{trans-[Fe}^{\text{II}}(\text{Py})_4(\text{NCE})_2]$ E = S or Se, see Experimental Section.

The metal complexes were characterised by standard techniques, single crystal X-ray crystallography, except for complex **1a**, and magnetic measurements. In Table 1 a summary of diagnostic IR vibrations is shown, demonstrating that in all cases the NCE co-ligands are coordinated through the N-atom.^[33–36] In the case of the symmetric *trans* complexes (**1a–b**), there is only one $\nu \text{N}=\text{C}(\text{E})$ (E = S, Se) band in the IR spectra, expected for this type of isomers, whereas for the *cis* complexes **2a** and **2b** there are two bands, but for complex **2c** only one band is observed.

X-ray crystallography

Single crystal X-ray diffraction data set was acquired at room and low temperature for all complexes on the same crystal, except for complex **1b** which was collected only at 199 K, due to a technical difficulty on the diffractometer cooling system, and due to the stabilisation of the HS-state at such temperature the

room temperature data set was not further pursued. Relevant bond lengths and angles, and single crystal data and structure refinement parameters for the iron(II) complexes are shown in Tables 2 and S1–S5 (CCDC: 2005424, 2005425, 2005427, 2005430, 2005431, 2005432 and 2005433). Complex **1b** crystallised in the $C2/c$ space group, Figure 5 and S16. Complex **2a** crystallised in the $P2_1/c$ space group, Figure 6, while complexes **2b** and **2c** are isostructural and isomorphs, crystallizing in the $P\bar{1}$ space group, Figures 6 and S17. Except for complexes **2b** and **2c**, all of them are solvent free. The asymmetric unit of complex **1b** comprises half complex molecule. The asymmetric unit of complex **2a** comprises one complex molecule at both acquisition temperatures (298(2) and 177(2) K), whilst **2b** shows two molecules independent by symmetry and half acetonitrile molecule solvent at both acquisition temperatures 298(2) and 177(2) K. However, at both temperatures the crystal structure of **2b** showed disordered solvent molecules that could not be appropriately modelled, thus the SQUEEZE^[37] routine in PLATON was performed, removing their contribution to the overall intensity data. An improvement was observed in the final refinement parameters and the electron density removed was in accordance with acetonitrile molecules (see supporting information), thus the formula from X-ray at both temperatures is $2\text{b}\cdot 1\frac{1}{4}\text{MeCN}$. Complex **2c** also shows two molecules independent by symmetry and one and a quarter acetonitrile molecule at 298(2) K, but two complex molecules independent by symmetry and half acetonitrile molecule at 175(2) K, suggesting a loss of solvent, however, there was disordered solvent molecules that could not be appropriately modelled at 175(2) K, thus the SQUEEZE^[37] routine in PLATON was performed, removing their contribution to the overall intensity data. An improvement was observed in the final refinement parameters and the electron density removed was in accordance with acetonitrile molecules (see supporting information), thus the formula for this complex is $2\text{c}\cdot 1\frac{1}{4}\text{MeCN}$ at both temperatures.

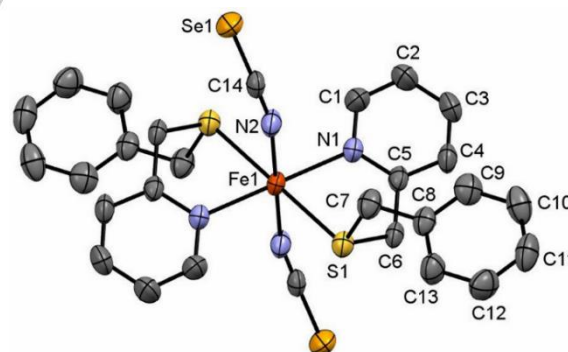


Figure 5. Perspective view of complex $\text{trans-[Fe}^{\text{II}}(\text{PySBn})_2(\text{NCSe})_2]$ (**1b**) acquired at 199(2) K. Ellipsoids are drawn at the 50 % probability level. Hydrogen atoms are omitted for the sake of clarity.

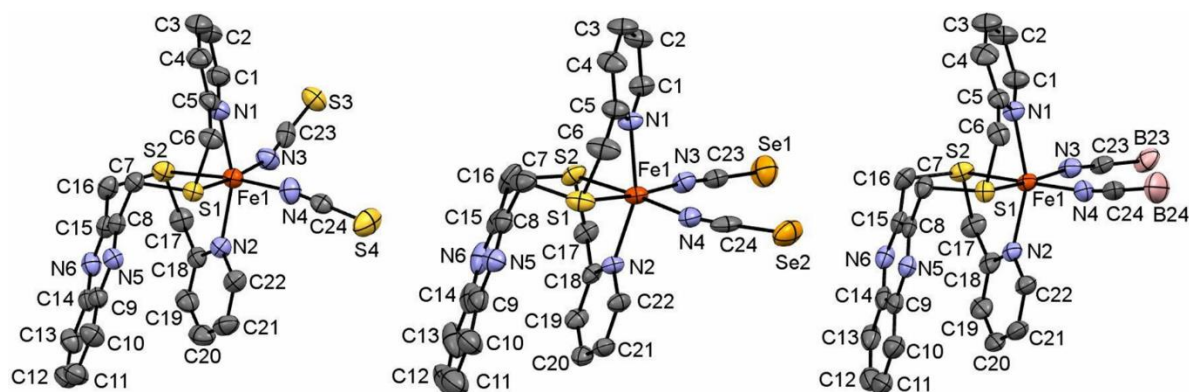


Figure 6. Perspective view of the family complex $cis\text{-}[\text{Fe}^{\text{II}}(\text{QuinoxS})(\text{NCE})_2]$ $E = \text{S, Se and BH}_3$; complexes (**2a**), (**2b**) and (**2c**) acquired at 177(2) K, 177(2) K and 175(2) K; left, centre and right respectively. Ellipsoids are drawn at the 50 % probability level. Hydrogen atoms and acetonitrile solvent molecules are omitted for the sake of clarity.

Table 2. Average bond distances (Å) and angles (°) and Σ_{Oh} parameter for the complex families **1** and **2**.

Complex	1b	2a	2b	2c
Temperature (K)	199(2)	177(2)	177(2)	175(2)
Space group	<i>C2/c</i>	<i>P2₁/c</i>	<i>P-1</i>	<i>P-1</i>
Av. Fe-N _{Py} (Å)	2.182(4)	2.177(4)	2.094(8)	2.127(6)
Av. Fe-N _{NCE} (Å)	2.105(4)	2.094(4)	2.091(10)	2.107(7)
Av. Fe-S (Å)	2.6004(13)	2.5964(13)	2.6044(32)	2.5899(23)
<i>trans</i> -N _{Py} -Fe-N _{Py} (°)	180.00	158.70(10)	156.59(23)	158.87(17)
<i>trans</i> -N _{NCE} -Fe-N _{NCE} (°)	180.00	-	-	-
Av. <i>trans</i> -S-M-N _{NCE} (°)	-	172.505(13)	173.20(29)	172.00(20)
<i>trans</i> -S-Fe-S (°)	180.00	-	-	-
Av. <i>cis</i> -N-Fe-N (°)	90.00(21)	96.56(26)	96.96(54)	95.99(38)
Av. <i>cis</i> -S-Fe-S (°)	-	99.28(3)	101.37(7)	101.81(6)
Av. <i>cis</i> -N-Fe-S (°)	90.00(23)	83.35(20)	82.81(43)	83.62(30)
Av. Fe-N-C(E) (°)	155.30	161.1	163.4	166.5
$\Sigma_{\text{Oh}}^{\text{[a]}}$	81.02(44)	82.00(33)	89.32(69)	80.06(67)

Av. = average, Py = pyridine, ^[a] The octahedral distortion parameter, Σ_{Oh} , is defined as the sum of the absolute values of the difference of each of the twelve *cis* angles from 90°. $\Sigma_{\text{Oh}} = 0$ indicates a perfect octahedral geometry.^[38,39]

In the crystal structures of **1b** it is possible to observe that the iron(II) centre is bonded to two **PySBn** bidentate ligands, in an all *trans* fashion, that is all the identical donors are found *trans* to each other, where the NCS_E co-ligands are found in apical positions, resulting in a distorted N₄S₂ octahedral geometry. Moreover, the bidentate ligand strands produce five-membered

metallocycles upon coordination. On the other hand, the complexes containing the tetradentate ligand **QuinoxS**, **2a-c**, also show a distorted N₄S₂ octahedral geometry for the iron(II) centre, but the NCE ligands are found in a *cis* coordination mode, instead of *trans* as **1b**. Due to the multidentate nature of the ligand, it is possible to identify a seven-membered and two five-membered metallocycles. There is no difference in the structural parameters found for complexes **2a-c** acquired at room and low temperature, suggesting that these complexes are not SCO-active.

Based on the data shown in Table 2, it is possible to observe that the structural data of the iron(II) complexes agree with the parameters found for related iron(II) complexes, $cis\text{-}[\text{Fe}^{\text{II}}(\text{bpte})_2(\text{NCE})_2]$, $\text{bpte} = \text{S,S}'\text{-bis}(2\text{-pyridylmethyl})\text{-1,2-thioethane}$, $E = \text{S, Se and BH}_3$,^[20,22] Table S7. The shortest bond type for all complexes comprises the Fe-N_{NCE} bond, as expected due to the anionic nature of the NCE co-ligands. The Fe-N bond length values agree for the high spin state stabilisation of the iron centre in all complexes (> 2.0 Å).^[40] Additionally, as expected, the Fe-S bonds are the longest bond type for all complexes.

The *cis* and *trans* bond angles for the thioether-complexes, **1b** and **2a-c**, are dispersed and away from the ideal values, 90 and 180 ° respectively, however, for complex **1b** the *trans* angle values are 180 °, which could be due to the all-*trans* geometry found for this complex and the fact that only a half complex molecule is found in the asymmetric unit, thus generating the other half by symmetry. The *cis* angles are found in a 78.1–101.9 and 77.8–102.7 ° range, for **1b** and **2a-c**, respectively. The *trans* angles for complexes **2a-c** range from 154.7 to 176.7 °. The more distorted *trans* angles correspond to the N_{Py}-Fe-N_{Py} angle, 154.7–159.9 °, whilst the N_{NCE}-Fe-S range from 169.0–176.7 °. The octahedral distortion parameter^[38,39] (Σ_{Oh}) values are found within the 80.06–91.58 ° range (see Tables 2 and S5) which is in perfect agreement with the high-spin state^[40] assignment based on the Fe-L bond lengths.

Finally, an analysis of the supramolecular interactions present in all the crystal structures reported in this work can be found in the supporting information, see page S19, that correspond to $\pi\text{-}\pi$ interactions $\text{CH}\cdots\pi$, and $\text{CH}\cdots\text{E}$ bonds.

Magnetic properties

All complexes were characterised by VT-magnetic studies in the solid state under a 0.1 T external magnetic field, in the 300 to 5 K temperature range at a 5 K min⁻¹ scan rate. The magnetic properties were acquired using either crystalline or powder samples. The crystalline samples, same sample used for SC-XRD, correspond to complexes **2a-c**, whereas the powder sample correspond to complex **1a-b**, either because of a small quantity was obtained from crystallization or no crystals could be grown at all. In Figures 7 and 8 the effective magnetic moment (μ_{eff}) vs. temperature (K) profile is shown, and in Table 3 a summary of the μ_{eff} values at room temperature and 50 K is presented.

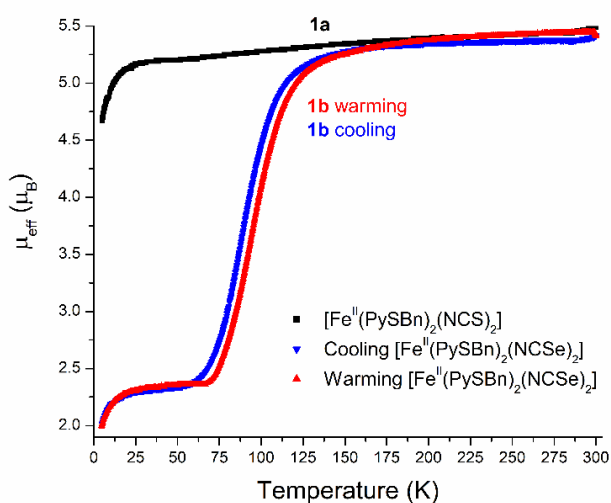


Figure 7. VT-magnetic behaviour for complexes **1a** and **1b** in the 300–5 K temperature range at 0.1 T external magnetic field and a 5 K min⁻¹ scan rate. The cooling (blue ▼) and warming (red ▲) behaviour for **1b** is shown.

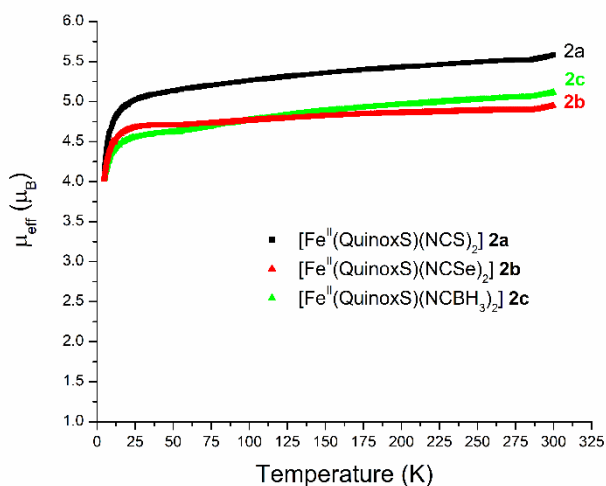


Figure 8. VT-magnetic behaviour for complexes **2a-c** in the 300–5 K temperature range at 0.1 T external magnetic field and a 5 K min⁻¹ scan rate.

All metal complexes are stabilised in the HS-state along the entire experimental temperature range, except for complex **1b** which shows spin crossover behaviour (see below). At room temperature the complexes stabilised in the HS-state show a μ_{eff}

value ranging from 4.9 to 5.5 μ_{B} , although for the majority of complexes the value is higher than the expected $\mu_{\text{S.O.}} = 4.9 \mu_{\text{B}}$, it is still in good agreement with the high spin state and suggests a considerable orbital contribution to g ,^[22,27,41] in addition the values are in agreement with the literature.^[20,42–44] The room temperature μ_{eff} value for complex **1a** containing the **PySBn** ligand (Figure 7) indicates that it is stabilised in the HS-state, the μ_{eff} value is maintained relatively constant down to 25 K, below this temperature zero field splitting (ZFS) is evident. Finally, for the complexes containing **QuinoxS** ligand (**2a-c**, Figure 8), μ_{eff} ranges from 4.9–5.6 μ_{B} , observing a decrease below c.a. 25 K due to ZFS.

Table 3. Effective magnetic moment for all metal complexes at 300 and 50 K, and spin state assignment.

Complex	μ_{eff} at 300 K (μ_{B})	μ_{eff} at 50 K (μ_{B})	Comments
1a	5.5	5.2	High spin
1b	5.4 ↓ / 5.4 ↑	2.3 ↓ / 2.4 ↑	Relatively abrupt, incomplete and hysteretic spin crossover
2a	5.6	5.1	High spin
2b	4.9	4.7	High spin
2c	5.1	4.6	High spin

Complex **1b** is the only one showing SCO behaviour, Figure 7. Complex **1b** is stabilised in the pure HS-state at 300 K with 5.4 μ_{B} , this value is relatively constant down to 150 K. A relatively abrupt decrease of the magnetic moment is observed below 140 K, reaching a plateau of 2.3–2.4 μ_{B} between 50–20 K, that is a c.a. 20 % of the iron centres are locked in the HS-state, considering the value of 5.4 μ_{B} at 300 K for the pure HS-state and 0 μ_{B} for the LS-state,^[45] indicating an incomplete transition in the lower temperature range. Below 20 K a sharp decrease is observed due to ZFS of the remaining HS-state. A cooling transition temperature ($T_{1/2\downarrow}$) of 92 K can be obtained from the first derivative of the spin transition curve. Upon warming, a similar behaviour is observed, however, the warming transition temperature ($T_{1/2\uparrow}$) is 98 K, that is a hysteresis loop width ($\Delta T_{1/2}$) of 6 K is observed. To ensure that the hysteresis loop is real, the magnetic profile was acquired at 1, 5 and 10 K min⁻¹ rate, Table 4 and Figures S23 and S24. At the slowest scan rates, 1 and 5 K min⁻¹, the hysteresis loop is not affected, $\Delta T_{1/2} = 5$ and 6 K, respectively, but at 10 K min⁻¹ the width increases to 11 K, in good agreement with the literature showing that at the fastest scan rates the hysteresis loop should be the widest,^[46–48] therefore confirming the hysteretic profile.

Table 4. Hysteresis loop scan rate dependence for complex **1b**.

Scan rate (K min ⁻¹)	$T_{1/2\downarrow}$ (K) ^[a]	$T_{1/2\uparrow}$ (K) ^[a]	$\Delta T_{1/2}$ (K)
1	93	98	5
5	92	98	6
10	91	102	11

^[a] Obtained from the first derivative of the spin transition curve.

Discussion

The differing magnetic behaviour of the metal complexes can be explained based on the electronic and structural differences among them. Two main differences among these complexes can be observed, the metallacycle size and the positioning of the co-ligands, *cis* vs. *trans*. The coordination mode of the NCE co-ligands seems not to have a direct influence on the magnetic properties of the complexes. In the previously reported SCO-active iron(II) complexes in N_4S_2 octahedral geometry, it was found that they contain such co-ligands in a *cis*-fashion,^[20,22] whilst the SCO-active complexes reported in this work are found in a *trans*-mode. The complexes containing the **QuinoxS** ligand (**2a-c**) comprise two five-membered and one seven-membered metallacycles, in addition an electron withdrawing quinoxaline moiety is present. These structural properties result in a weak field ligand, and HS-only iron(II) complexes. Nonetheless, one of the two complexes based on **PySBn** ligand is SCO-active, **1b**. The presence of five-membered metallacycles and a good π -acid thioether ligand, that can stabilise the LS-state due to $d\pi-d\pi$ back bonding,^[49-51] permit the modulation of the crystal field by co-ligands and conferring a stronger field (NCE, E = Se), producing in this way a SCO-active compound. Complex **1b** shows a relatively abrupt hysteretic SCO.

The sample used for the magnetic measurements for the SCO-active complex was in powder form, obtained by precipitation from the reaction mixture, although it was possible to obtain crystals for complex **1b**, the amount was only enough for SC-XRD. Therefore, the hysteretic magnetic profile for **1b** is surprising, because, as it is known, the systems possessing high cooperativity within the crystal structure are more likely to show hysteresis, as in most of the crystalline samples; while in powders the supramolecular interactions responsible for the cooperativity may be debilitated.^[47,52,53] Although, the sample used for the magnetic measurements is different from the crystals used for SC-XRD, it is interestingly to note that the supramolecular interactions present in the crystal structure at 199(2) K are actually medium to weak slipped π - π stackings and non-classical C-H...Se bonds, Figure **S18**. The former interaction occurs between a pyridine ring of a complex molecule and the pyridine ring of a neighbouring molecule, where the aromatic rings are almost coplanar with an angle between the plane formed by both pyridine rings of 3.6°, whereas the distance between both centroids is 3.64 Å. The second type of interaction occurs between the *para* carbon of the benzyl group of a complex molecule and the Se-CN of a neighbouring molecule, a C...Se distance of 3.92 Å is found. The latter molecule shows the same interaction with a neighbouring molecule, but interacting through the benzyl group, producing a 1D supramolecular polymer that is intertwined with neighbouring chains by the above mentioned pyridyl-pyridyl π - π interactions forming 2D sheets, thus is highly likely that the powder and crystalline samples possess the same interactions that promotes cooperativity and thus hysteresis in the magnetic profile.

Brooker and co-workers^[36] have shown that the Fe-N-C(E) (E = S, Se or BH₃) bond angle is diagnostic for determining the spin lability of the metal complexes for a family of structurally characterised iron(II) complexes containing 3-pyridyl-4-substituted-1,2,4-triazoly ligands (Rdpt) and NCE co-ligands in N₆ coordination sphere. The SCO-active complexes showed an angle range of 162–178°, whilst the range found for the HS-locked complexes is 142–159°. It is clear that the SCO-active

complexes show Fe-N-C(E) angles closer to 180°. It is important to note that there is a small number of SCO-active complexes possessing N₄S₂ coordination sphere and containing NCE co-ligands,^[20,22] however, an analysis of the Fe-N-C(E) (E = S, Se or BH₃) bond angle range obtained from X-ray crystallography for the complexes reported in this work and those reported in the literature for the SCO-active complexes *in the HS-state* varies as follows (Figure **10**): for the SCO-active complexes the experimental ranges observed are 165.9° for S (only one complex has been reported), whereas for Se and BH₃ the ranges are 155.3–176.3 and 161.9° (only one complex), respectively. In the case of the HS-only complexes the angle range at room temperature is 152.0–170.2, 150.0–168.6 and 161.4–172.7° for S, Se and BH₃, respectively. Due to the small number of examples is difficult to find a trend, particularly for the S- and BH₃-based complexes, which only one complex is SCO-active of each. Nonetheless, for the Se-based complexes the angle range for the SCO-active complexes is closer to linearity than the HS-only complexes that show smaller angles.

In addition, we have analysed other structural features closely related to the Fe-N-C(E) angle such as the (N)C—E and N—C(E) bond lengths and the N-C-E angle of the co-ligands, Figure **10** and Tables **S8** and **S9**. The ranges for the (N)C—E and N—C(E) bond lengths for the SCO-active complexes, *in the HS state*, corresponding to the S, Se and BH₃ anions are 1.618 (only one complex), 1.765–1.803 and 1.583 Å (only one complex), and 1.158 (only one complex), 1.108–1.165 and 1.141 (only one complex) Å, respectively. The range for the (N)C—E bond lengths in the case of the HS-only complexes, at room temperature, show a range of 1.622–1.648, 1.713–1.799, 1.564–1.577 Å, whilst the N—C(E) bond length varies 1.097–1.129, 1.093–1.166 and 1.121–1.134 Å for S, Se and BH₃, respectively. Whereas the N-C-E angle of the co-ligands for the SCO-active complexes, in the HS-state, range is as follow: 179.6 (only one complex), 177.2–179.3 and 177.5° (only one complex), and the range for HS-only complexes, at room temperature, are 178.2–178.6, 176.9–179.4 and 176.7–179.0° for S, Se and BH₃, respectively. In the case of the (N)C—E bond length, there is no clear difference between the SCO-active and the HS-only complexes. In the case of the N—C(E) bond length value ranges, at least for the S and BH₃-based complexes, indicate that in the SCO-active complexes the N—C bond elongates in comparison to the HS-only complexes, suggesting a much more electron density donation towards the metal centre, debilitating the N—C bond in SCO-active complexes. The N-C-E angle trend is like the one found for Fe-N-C(E), that is the angle in the SCO-active complexes is closer to linearity than the HS-only complexes, except for the NCBH₃ anion that have smaller angle values. Thus, from these results it seems that the more diagnostic parameters to evaluate spin lability are the Fe-N-C(E) angle and N—C(E) bond length values, Figure **9**. A plot of these two parameters shows that the N—C(E) bond length value is a better marker for determining the probability of observing the SCO effect, as the complexes with longer values are SCO-active. From Figure **9** it is possible to observe that 10 out of 14 complexes that have a bond length larger than 1.14 Å are SCO-active, that is a 71%. It is important to mention that there are just a few of SCO-active complexes, compared to HS-only, which could hamper an in depth analysis and to establish an accurate bond length and angle range for

determining spin lability of an iron(II) complex based on structural parameters for this type of S-containing complexes.

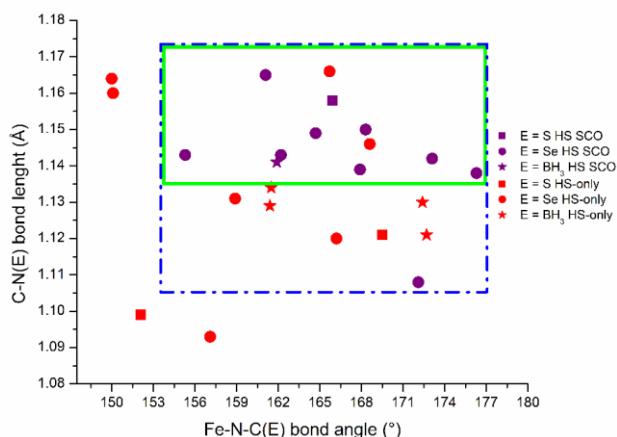


Figure 9. Fe-N-C(E) angle vs. N—C(E) bond length values plot. The blue dotted box highlights the area where all the SCO-active complexes can be found, and the green solid box shows the highest density of SCO-active complexes showing higher Fe-N-C(E) angles and N—C(E) bond length values than the HS-only complexes. The SCO-active complexes are shown in purple symbols, and the HS-only complexes are shown in red symbols.

Conclusion

The ligands containing thioether functional groups can produce SCO-active complexes, as previously reported by other authors. However, we have shown that the chelate ring size and the selection of NCE co-ligands are important for tuning the crystal field adequately but are not the only factors. The packing interactions in the resulting metal complexes is quite important as the presence/absence of solvent molecules can promote or deactivate SCO, polymorphism, or other crystallographic phenomena. In addition, the nature of the substituents on the ligand scaffold, is important as well, see below. In the case of **PySBn** ligand, it forms five-membered metallacycles, and can

produce SCO-active complexes in combination with a right co-ligand. The NCSe-based complex **1b** shows a relatively abrupt and hysteretic SCO profile, whereas the magnetic profile for the NCS complex **1a** is in agreement for a complex stabilised in the HS-state. In contrast, the tetra-dentate ligand **QuinoxS** produced HS-only complexes, being the main differences with the **PySBn**-based complexes the combination of five- and seven-membered rings present in the complexes of the former ligand, and the electron withdrawing quinoxaline heterocycle. Another important difference is the disposition of the NCE co-ligands, for the **QuinoxS** complexes the co-ligands are in a *cis*-manner but in the **PySBn** complexes the disposition is *trans*, however both types of complexes can be SCO-active, for example the family *cis*-[Fe^{II}(bpte)(NCE)₂] and complex *trans*-**1b**. An analysis of the structural parameters of the complexes reported in this work and literature-based SCO-active complexes with N₄S₂ coordination spheres containing NCE co-ligands demonstrated, as previously reported, that the Fe-N-C(E) bond angle is a suitable parameter for determining the potential SCO-character of a complex, as in the SCO-active complexes such angle is usually almost linear, close to 180°. In addition, we have demonstrated that the N—C(E) bond length is as well a suitable parameter when considering the feasibility of SCO, as in SCO-active complexes such bond is longer than for HS-only complexes, N—C(E) bond > 1.14 Å.

Finally, we have shown that readily available and simple thioether based complexes can produce SCO-active complexes with hysteresis, the latter property is actually not easy to achieve, and in our case, it is observed in powder materials, which is important due to the difficulty of obtaining crystalline materials. Therefore, our work has expanded the ligand repertoire of S-based ligands that produce SCO-active materials, that can be easily modified to tune the magnetic properties by introducing different N-heterocycles on one arm and electron-donating/withdrawing substituents on the other arm of the thioether group, which can positively impact the magnetic properties.

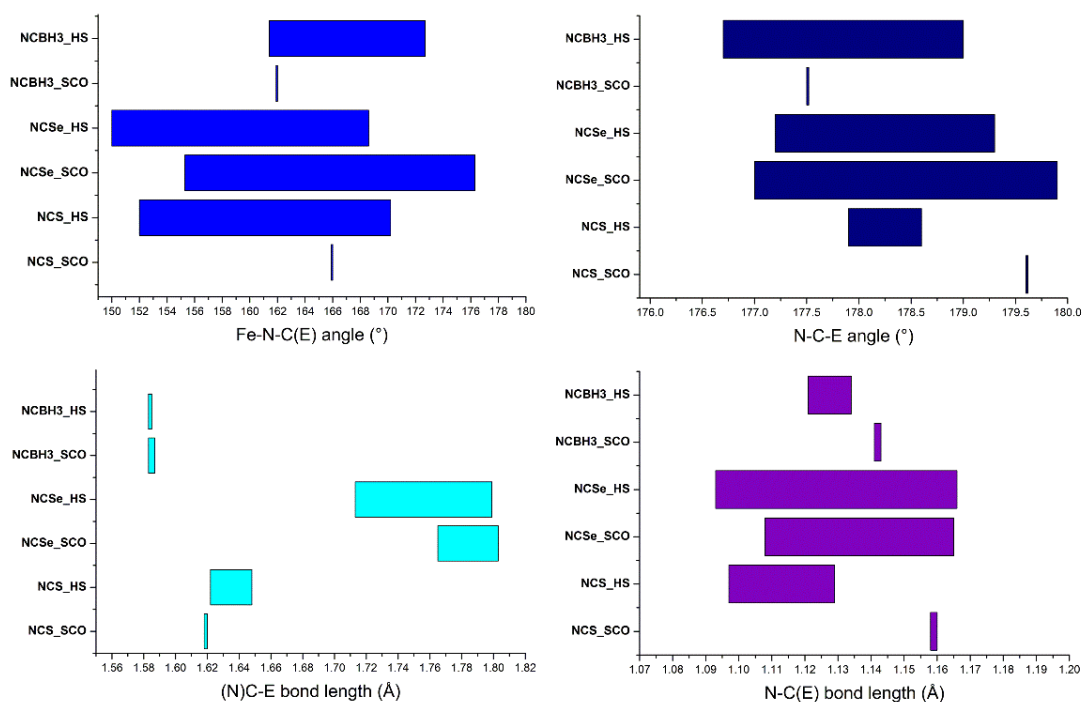


Figure 10. Bar plots for the Fe-N-C(E) and N-C-E bond angle range (top) and for the (N)C-E and N-C(E) bond length range (bottom) for SCO-active and HS-locked complexes of the type $[\text{Fe}^{\text{II}}(\text{N}_2\text{S}_2)(\text{NCE})_2]$.

Experimental Section

General

All reactions were carried out under argon atmosphere using standard Schlenk techniques. Solvents were purified and dried by standard procedures (tetrahydrofuran over Na/benzophenone, methanol and ethanol over Mg/I₂, acetone and acetonitrile over P₂O₅) and were distilled under argon prior to use. All other chemicals were used as purchased from Sigma-Aldrich, Merck, and J. T. Baker. Column chromatography was carried out utilising Sigma-Aldrich Silica Gel (40–63 μm particle size). TLC was performed with Macherey-Nagel Alugram@Xtra Sil G/UV₂₅₄ plates employing UV light for visualization. All compressed gases were obtained from Infra. Argon (> 99.9 %) and nitrogen (> 99.5 %) were used as supplied without purification. FT-IR spectra were recorded utilising a FT-IR Perkin Elmer Spectrum GX as KBr pellets (4000–400 cm⁻¹) and utilizing a Varian 640-IR Spectrometer with Attenuated Total Reflectance (ATR) (4000–500 cm⁻¹). The ¹H (300, 400 and 500 MHz), ¹³C{¹H} (75, 101 and 126 MHz) spectra were recorded in either a Bruker Advance DPX 300 MHz, Jeol Eclipse 400 MHz or Jeol Eclipse ECA 500 MHz at room temperature. ¹H and ¹³C{¹H} spectra are referenced internally using the residual proton and carbon solvent resonances relative to tetramethylsilane. High-resolution mass spectra (HRMS) were obtained by HPLC 1100 coupled/MSD-TOF with APCI as ionization source in an Agilent Technologies HR-MSTOF G1969A. Mass spectra were obtained on an Agilent HPLC-SQ-MS, HPLC 1200 series and MS-ESI-SQ model 6120. Elemental analyses were performed on a Thermo-Finnigan Flash 1112 elemental analyser in the Chemistry Department at CINVESTAV.

Magnetic measurements

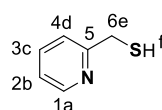
The magnetic susceptibility measurements were carried out on a Quantum Design Physical Property Measurement System (PPMS) Dynacool-9T equipped with a vibrating sample mount (VSM). The measurements were performed in the temperature range of 300–5 K and at 5 K min⁻¹ rate with an applied field of 0.1 T (1000 Oe). Microcrystalline or powder samples of complexes **1a–b** and **2a–c** were employed in the measurements. In addition, the magnetic data for complex **1b** was

collected at 1 and 10 K min⁻¹ rates. Data were corrected for the diamagnetism of the sample.

X-ray crystallography

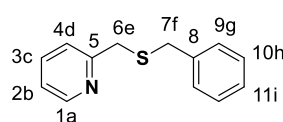
X-ray diffraction measurements were collected on a Bruker APEX-II CCD diffractometer, using graphite-monochromated Mo K α radiation ($\lambda = 0.71073$ Å). The structures were solved by direct methods, using SHELXS-2014 included in WinGX v.2014.1 and refined by a full-matrix least-squares method based on F₂.^[54] Absorption corrections were performed by Multi-Scan. All non-hydrogen atoms were refined with anisotropic thermal displacement coefficients unless specified otherwise. Due to badly disordered solvent molecules in complexes **2b** and **2c** the SQUEEZE^[37] routine in PLATON was performed removing its contribution to the overall intensity data. An improvement was observed in the final refinement parameters. For more details of the structure refinement of complexes **2b** and **2c** see supporting information. The crystallographic information file (CIF) for compounds **1b** and **2a–c** (CCDC: 2005424, 2005425, 2005427, 2005430, 2005431, 2005432 and 2005433) contains the supplementary crystallographic data for this paper.

Synthesis

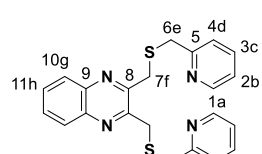


2-Pycolythiol (B¹). The synthesis of **B¹** was based on the literature with slight modifications.^[30] In a 100 mL round-bottom flask under argon atmosphere 2-(chloromethyl)pyridine hydrochloride (3.000 g, 18.288 mmol, 1 eq.), thiourea (1.520 g, 20.117 mmol, 1.1 eq.) and 50 mL of distilled and degassed water were added. The resulting orange solution was heated to 80–85 °C for 1 h. Once the amber solution reached room temperature it was cooled to 0 °C, followed by addition of sodium hydroxide (2.340 g, 58.530 mmol, 3.2 eq.). The resulting mixture was stirred for 30 minutes at 0 °C followed by further stirring at room temperature for 12 h, before the yellowish solution was extracted with 200 mL of diethyl ether. The basic aqueous phase was cooled to 0 °C and neutralised by careful dropwise addition of a hydrochloric acid solution (37 %, w/w) until obtaining a pH value of 7.

Then, the neutralised aqueous phase was extracted with 200 mL of diethyl ether, and the combined organic extracts were dehydrated with sodium sulphate, filtered and the solvent was removed in vacuo, to afford **B**¹ (1.442 g, 11.522 mmol, **63** %) as a yellow oil, which was used in next synthetic step without further purification. The spectroscopic data were in good agreement with the literature.^[55] ¹H-NMR (300 MHz, CDCl₃ @ 7.26) δ 8.54 (d, J = 4.3 Hz, 1H, H_a), 7.65 (td, J = 7.8, 1.7 Hz, 1H, H_c), 7.33 (d, J = 7.8 Hz, 1H, H_d), 7.16 (t, J = 7.0 Hz, 1H, H_b), 3.85 (d, J = 7.9 Hz, 2H, H_e), 2.03 (t, J = 7.7 Hz, 1H, H_f). ¹³C{¹H}-NMR (126 MHz, CDCl₃ @ 77.16) δ (ppm): δ 160.25 (5), 149.54 (1), 137.02 (3), 122.41 (2), 122.08 (4), 30.95 (6).



Benzylpicolythioether (PySBn). The synthesis of **PySBn** was based on the literature with slight modifications.^[29] A Schlenk flask under argon atmosphere was charged with **B**¹ (1.442 g, 11.252 mmol, 1 eq.), benzyl chloride (1.29 mL, 11.252 mmol, 1 eq.), sodium hydroxide (450 mg, 11.252 mmol, 1 eq.) and 100 mL of anhydrous and degassed ethanol. The resulting pale-yellow solution was heated to reflux for 12 h. After that time, the resulting amber mixture was cooled to room temperature, and filtered. The solution was then extracted with 200 mL of dichloromethane, and the combined organic phases were dehydrated with sodium sulphate, filtered, and the solvent was removed in vacuo to afford **PySBn** as a reddish oil (2.205 g, 10.239 mmol, **91** %), which crystallized at 0–5 °C as prismatic red crystals. ¹H-NMR (500 MHz, CDCl₃ @ 7.26) δ 8.55 (dd, J = 4.8, 0.8 Hz, 1H, H_a), 7.62 (td, J = 7.7, 1.7 Hz, 1H, H_c), 7.39–7.28 (m, 3H, H_d, H_g y H_h), 7.26–7.21 (m, 1H, H_i), 7.15 (dd, J = 7.4, 4.9 Hz, 1H, H_b), 3.75 (s, 2H, H_e), 3.69 (s, 2H, H_f). ¹³C{¹H}-NMR (126 MHz, CDCl₃ @ 77.16) δ (ppm): 158.67 (5), 149.41 (1), 138.12 (8), 136.70 (3), 129.12 (9), 128.55 (10), 127.07 (11), 123.20 (4), 121.94 (2), 37.57 (6), 35.96 (7). IR-ATR v (cm⁻¹): 3055 (w), 2967 (w), 1588 (m), 1563 (m), 1493 (m), 1467 (m), 1452 (m), 1431 (s), 1306 (w), 1423 (w), 1216 (w), 1146 (w), 1088 (m) 1069 (m), 1043 (m), 1206 (m), 994 (m), 926 (w), 903 (w), 791 (m), 770 (m), 745 (s), 705 (s), 669 (m), 629 (w), 579 (m), 562 (m). SQ-ESI(+)/MS (m/z) MeCN: Calculated for [C₁₃H₁₄NS]⁺ 216.1, found 216.1.



2,3-bis((2-picolyl)thio)methyl quinoxaline (QuinoxS). The synthesis of **QuinoxS** was based on the literature with slight modifications.^[31] A Schlenk flask under argon atmosphere was charged with 2,3-bis(bromomethyl)quinoxaline (1.487 g, 4.705 mmol, 1 eq.), **B**¹ (1.178 g, 9.411 mmol, 2 eq.), sodium hydroxide (376 mg, 9.411 mmol, 2 eq.) and 100 mL of anhydrous and degassed ethanol. The resulting brown solution was heated to reflux for 3 h. After cooling to room temperature, the solution was filtered off and extracted utilising 100 mL of distilled and degassed water and 200 mL of degassed dichloromethane. The combined organic extracts were dehydrated with sodium sulphate, and the solvent was removed in vacuo to provide a brownish solid, which was further purified by column chromatography on silica gel with dichloromethane/acetone gradient (100/0 to 75/25) as the eluent. The solvent was removed under reduced pressure to afford **QuinoxS** (1.638 g, 4.048 mmol, **86** %) as an off-white solid. ¹H-NMR (400 MHz, CDCl₃ @ 7.26) 8.49 (ddd, J = 4.9, 1.8, 0.9 Hz, 2H, H_a), 8.00 (dd, J = 6.3, 3.5 Hz, 2H, H_g), 7.70 (dd, J = 6.4, 3.4 Hz, 2H, H_h), 7.56 (td, J = 7.7, 1.8 Hz, 2H, H_c), 7.35 (d, J = 7.8 Hz, 2H, H_d), 7.08 (ddd, J = 7.5, 4.9, 1.1 Hz, 2H, H_b), 4.16 (s, 2H, H_f), 3.84 (s, 2H, H_e). ¹³C{¹H}-NMR (101 MHz, CDCl₃ @ 7.26) 158.00 (5), 152.47 (8), 149.72 (1), 140.86 (9), 136.62 (3), 129.68 (11), 128.89 (10), 123.37 (4), 122.05 (2), 37.98 (6), 35.45 (7). IR-ATR v (cm⁻¹): 3055 (w), 2971 (w), 2928 (w), 1584 (m), 1567 (m), 1479 (m), 1435 (m), 1415 (w), 1361 (w), 1325 (m), 1267 (w), 1180 (w), 1126 (w), 1051 (w), 995 (m), 937 (w), 898 (w), 830 (w), 805 (w), 788 (w), 732 (s), 746 (s), 709 (w), 683 (m), 614 (w), 581 (w), 557 (s). SQ-ESI(+)/MS (m/z) MeCN: Calculated for [C₂₂H₂₁N₄S₂]⁺ = 405.1, found 405.1.

Complex synthesis

Synthetic methodology for *trans*-[Fe^{II}(Py)₄(NCE)₂] E = S, Se, BH₃.

The synthesis of the complexes is based on reference.^[32] A Schlenk flask under argon atmosphere was charged with two equivalents of the corresponding cyano-derivative salt (NH₄NCS, KNCS or NaNCBH₃), which was dissolved in 30 mL of distilled and degassed water, followed by addition of six equivalents of pyridine. Under vigorous stirring, one equivalent of iron(II) chloride tetrahydrate salt was added, observing the instantaneous precipitation of yellow solids for NCS and NCBH₃ or olive green solid for NCSe derivatives. The corresponding resulting mixture was stirred at room temperature for 1 h. The resulting precipitate solid was filtered *via* cannula and washed with distilled and degassed water (3 x 50 mL) to remove pyridine excess. Finally, the solid was dried *in vacuo* affording the corresponding complex in **85** % (NCS, yellow), **70** %, (NCSe, olive green) and **95** % (NCBH₃, pale-yellow) yield. NCS: IR-ATR v (cm⁻¹): 2059 (s), 1597 (s), 1485 (m), 1440 (s), 1213 (w), 1147 (w), 1068 (m), 1038 (m), 1005 (m), 806 (w), 764 (m), 754 (m), 711 (s), 699 (s), 652 (w), 622 (m). NCSe IR-ATR v (cm⁻¹): 2060 (s), 1597 (s), 1484 (m), 1440 (s), 1356 (w), 1213 (m), 1147 (w), 1068 (m), 1038 (m), 1005 (m), 764 (m), 754 (m), 710 (s), 700 (s), 652 (w), 623 (m), 585 (m), 567 (m). NCBH₃ IR-ATR v (cm⁻¹): 2337 (m), 2179 (m), 1597 (m), 1486 (w), 1439 (m), 1217 (m), 1154 (w), 1120 (m), 1068 (w), 1039 (m), 1008 (m), 753 (m), 697 (s), 627 (m), 593 (w), 569 (s).

Synthetic methodology for complexes [Fe^{II}(L)_n(NCE)₂]

All the metal complexes were synthesised following two possible methodologies.

Method A: A Schlenk flask under argon atmosphere was charged with iron(II) chloride tetrahydrate (1 eq.), A[NCE] salt (2 eq., A = NH₄ for E = S, A = K for E = Se and A = Na for E = BH₃) and an adequate anhydrous and degassed solvent. The resulting solution was stirred for 1 h at room temperature and filtered *via* canula to remove inorganic salts. The filtrate solution was added *via* cannula to a solution of the corresponding ligand (1 or 2 eq.) in an adequate solvent. The mixture was stirred for 2 h at room temperature observing the precipitation of a solid. Finally, the solid was filtered *via* canula and dried under reduced pressure to afford the corresponding product as powders.

Method B: A Schlenk flask under argon atmosphere was charged with precursor complex [Fe^{II}(Py)₄(NCE)₂] (1 eq.) and 5 mL of anhydrous and degassed solvent. The resulting suspension was layered with fresh and degassed solvent. Finally, a solution of the corresponding ligand (1 or 2 eq.) in an adequate solvent was carefully deposited over the previous layers. The three layers were mixed by liquid-liquid slow diffusion over a few days, obtaining crystals.

Complex *trans*-[Fe^{II}(PySBn)₂(NCS)₂] (1a). **Method A:** iron(II) chloride tetrahydrate (92 mg, 0.465 mmol, 1 eq.), ammonium isothiocyanate (106 mg, 1.395 mmol, 3 eq.) and 10 mL of anhydrous and degassed ethanol were stirred at room temperature for 1 h then filtered to remove ammonium chloride and ammonium isothiocyanate excess. The purple solution was dried in vacuo to isolate bis-isothiocyanate iron(II) salt as a yellow solid, which was dissolved in 10 mL of anhydrous and degassed acetone, resulting in a purple solution. A pale-red solution of **PySBn** (200 mg, 0.930 mmol, 2 eq.) in 10 mL of anhydrous and degassed acetone was added *via* cannula. The resulting amber solution was stirred for 3 h at room temperature observing the precipitation of an off-white solid. The solid was filtered off *via* canula to afford complex **3a** (76 mg, 0.127 mmol, **27** %) as a white solid, which was dried under reduced pressure.

Modified method B: To a suspension of precursor complex [Fe^{II}(Py)₄(NCS)₂] (220 mg, 0.450 mmol, 1 eq.) in 10 mL of anhydrous and degassed ethanol was added a solution of **PySBn** (194 mg, 0.900 mmol, 2 eq.) in 5 mL of anhydrous and degassed ethanol *via* cannula resulting in a purple solution. After a few minutes, a white solid had precipitated, which was filtered off and dried *in vacuo* resulting in a white powder

(218.3 mg, 0.360 mmol, **80** %). **IR-ATR** ν (cm^{-1}): 2059 (s), 1598 (m), 1570 (w), 1478 (m), 1438 (m), 1309 (w), 1150 (w), 1098 (w), 1056 (w), 1017 (w), 964 (w), 910 (w), 841 (w), 774 (m), 752 (m), 711 (s), 699 (s), 674 (m), 641 (m), 624 (m), 593 (m), 567 (m). **SQ-ESI(+)**M/S (m/z) DMSO: Calculated for $[\text{Fe}^{\text{II}}(\text{C}_{13}\text{H}_{13}\text{NS})_2(\text{Cl})]^+$ 521.1, found 521.1. **Elemental analysis** (%): Calculated for $[\text{Fe}^{\text{II}}(\text{C}_{13}\text{H}_{13}\text{NS})_2(\text{NCS})_2]\cdot\text{H}_2\text{O}$ C: 54.19, H: 4.55, N: 9.03; found: C: 54.30, H: 4.26, N: 10.51.

Complex trans-[Fe^{II}(PySBn)₂(NCSe)₂] (1b). **Method A:** similar to complex **3a**, **PySBn** (200 mg, 0.930 mmol, 2 eq.), iron(II) chloride tetrahydrate (92 mg, 0.465 mmol, 1 eq.) and potassium isoselenocyanate (202 mg, 1.395 mmol, 3 eq.). Complex **3b** was isolated as a white solid (66 mg, 0.094 mmol, **20** %). **Modified method B:** similar to complex **3a**. Complex $[\text{Fe}^{\text{II}}(\text{Py})_4(\text{NCSe})_2]$ (125 mg, 0.216 mmol, 1 eq.) and **PySBn** (93 mg, 0.432 mmol, 2 eq.). Complex **3b** was isolated as pale grey solid (22 mg, 0.032 mmol, **15** %). Single crystals suitable for X-ray crystallography were obtained by diethyl ether vapor diffusion into the filtrate solution. **IR-ATR** ν (cm^{-1}): 3028 (w), 2059 (s), 1598 (m), 1568 (w), 1494 (m), 1476 (m), 1437 (m), 1416 (w), 1399 (w), 1308 (m), 1265 (w), 1246 (w), 1025 (w), 1149 (m), 1098 (m), 1055 (m), 1018 (m), 965 (w), 910 (m), 841 (m), 773 (s), 751 (s), 711 (s), 699 (s), 671 (m), 640 (m), 595 (m), 576 (m).

Complex cis-[Fe^{II}(QuinoxS)(NCS)₂] (2a). **Method B:** $[\text{Fe}^{\text{II}}(\text{Py})_4(\text{NCS})_2]$ (110 mg, 0.225 mmol, 1 eq.) in 10 mL of anhydrous and degassed acetonitrile. Over this solution 10 mL of anhydrous and degassed acetonitrile were carefully added, forming two liquid layers. A third liquid layer of a yellow solution of **QuinoxS** (100 mg, 0.225 mmol, 1 eq.) in 10 mL of anhydrous and degassed chloroform was carefully deposited over the previous layers. The three layers were mixed by liquid-liquid slow diffusion over 4 days, obtaining a pale red solution, and amber crystals with prismatic morphology of complex **4a** which were suitable for single crystal X-ray diffraction (53 mg, 0.092 mmol, **41** %). **IR-ATR** ν (cm^{-1}): 2070 (m), 2059 (m), 1600 (m), 1482 (m), 1439 (m), 1390 (d), 1359 (d), 1315 (d), 1265 (d), 1242 (d), 1201 (d), 1162 (d), 1125 (w), 1103 (w), 1052 (w), 1017 (m), 879 (w), 851 (w), 822 (w), 767 (s), 696 (w), 640 (m), 611 (m), 563 (s). **SQ-ESI(+)**M/S (m/z) DMF: Calculated for $[\text{Fe}^{\text{II}}(\text{C}_{22}\text{H}_{20}\text{N}_4\text{S}_2)(\text{NCS})_2]^+$ 518.0, found 518.1. **Elemental analysis** (%): Calculated for $[\text{Fe}^{\text{II}}(\text{C}_{22}\text{H}_{20}\text{N}_4\text{S}_2)(\text{NCS})_2]$ C: 50.00, H: 3.50, N: 14.58; found: C: 50.21, H: 3.30, N: 14.74.

Complex cis-[Fe^{II}(QuinoxS)(NCSe)₂] (2b). **Method B:** Similar to complex **4a**. $[\text{Fe}^{\text{II}}(\text{Py})_4(\text{NCSe})_2]$ (131 mg, 0.225 mmol, 1 eq.) in 10 mL of acetonitrile. Layered with a solution of **QuinoxS** (100 mg, 0.225 mmol, 1 eq.) in 10 mL of CHCl_3 . Complex **4b** was obtained as prismatic yellow crystals (59 mg, 0.101 mmol, **57** %). **IR-ATR** ν (cm^{-1}): 2061 (w), 1650 (w), 1595 (w), 1476 (w), 1441 (w), 1342 (w), 855 (w), 758 (m), 700 (w), 646 (w), 609 (m), 584 (m), 550 (s). **SQ-ESI(+)**M/S (m/z) DMSO: Calculated for $[\text{Fe}^{\text{II}}(\text{C}_{22}\text{H}_{20}\text{N}_4\text{S}_2)(\text{Cl})]^+$ 495.0, found 495.0.

Complex cis-[Fe^{II}(QuinoxS)(NCBH₃)₂] (2). **Method B:** Similar to complex **4a**. $[\text{Fe}^{\text{II}}(\text{Py})_4(\text{NCBH}_3)_2]$ (102 mg, 0.225 mmol, 1 eq.) in 10 mL of acetonitrile. Layered with a solution of **QuinoxS** (59 mg, 0.101 mmol, 2 eq.) in 10 mL of CHCl_3 . Complex **4c** was obtained as prismatic yellow crystals (59 mg, 0.101 mmol, **45** %). **IR-ATR** ν (cm^{-1}): 2349 (m), 2179 (m), 1601 (m), 1587 (w), 1483 (m), 1438 (m), 1392 (w), 1360 (w), 1268 (w), 1114 (m), 1057 (w), 1019 (w), 851 (w), 759 (s), 694 (w), 642 (w), 592 (s), 574 (s), 564 (s). **SQ-ESI(+)**M/S (m/z) DMF: Calculated for $[\text{Fe}^{\text{II}}(\text{C}_{22}\text{H}_{20}\text{N}_4\text{S}_2)(\text{NCBH}_3)_2]^+$ 500.1, found 500.1. **Elemental analysis** (%): Calculated for $[\text{Fe}^{\text{II}}(\text{C}_{22}\text{H}_{20}\text{N}_4\text{S}_2)_2(\text{NCBH}_3)_2]\cdot(\text{CH}_3\text{CN})$ C: 53.74, H: 5.03, N: 16.87; found: C: 53.22, H: 5.14, N: 17.41.

Acknowledgements

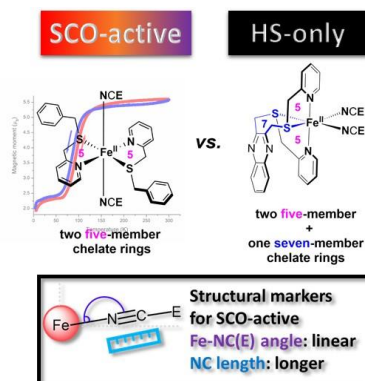
This work was financially supported by CINVESTAV and SEP-CONACyT (CB 2016/286346). Diego Plaza-Lozano thanks CONACyT for a PhD scholarship (Beca 591879).

Keywords: Spin crossover • Magnetic properties • iron(II) compounds • S-based ligands • Hysteresis

- [1] P. Gütllich, H. A. Goodwin, in *Spin Crossover Transit. Met. Compd. I* (Eds.: P. Gütllich, H.A. Goodwin), Springer Berlin Heidelberg, Berlin, Heidelberg, **2004**, pp. 1–47.
- [2] J. A. Real, A. B. Gaspar, M. C. Muñoz, *Dalton Trans.* **2005**, 2062–2079.
- [3] M. A. Halcrow, Ed., *Spin-Crossover Materials: Properties and Applications*, John Wiley & Sons, Ltd, **2013**.
- [4] O. S. Zhao-Yang Li, Z.-S. Yao, S. Kang, S. Kanegawa, in *Spin-Crossover Mater.* (Ed.: M.A. Halcrow), John Wiley & Sons, Ltd, **2013**.
- [5] J.-F. Létard, P. Guionneau, L. Goux-Capes, in *Spin Crossover Transit. Met. Compd. III*, Springer Berlin Heidelberg, Berlin, Heidelberg, **2004**, pp. 221–249.
- [6] S. Brooker, J. A. Kitchen, *Dalton Trans.* **2009**, 7331–7340.
- [7] A. Bousseksou, G. Molnár, L. Salmon, W. Nicolazzi, *Chem. Soc. Rev.* **2011**, *40*, 3313–3335.
- [8] H. Li, H. Peng, *Curr. Opin. Colloid Interface Sci.* **2018**, *35*, 9–16.
- [9] G. Molnár, S. Rat, L. Salmon, W. Nicolazzi, A. Bousseksou, *Adv. Mater.* **2018**, *30*, 1703862.
- [10] G. Molnár, L. Salmon, W. Nicolazzi, F. Terki, A. Bousseksou, *J. Mater. Chem. C* **2014**, *2*, 1360–1366.
- [11] R. Pei, E. Matamoros, M. Liu, D. Stefanovic, M. N. Stojanovic, *Nat. Nanotechnol.* **2010**, *5*, 773.
- [12] R. N. Muller, L. Vander Elst, S. Laurent, *J. Am. Chem. Soc.* **2003**, *125*, 8405–8407.
- [13] J. Olguin, *Coord. Chem. Rev.* **2020**, *407*, 213148.
- [14] D. J. Harding, P. Harding, W. Phonsri, *Coord. Chem. Rev.* **2016**, *313*, 38–61.
- [15] H. A. Goodwin, in *Spin Crossover Transit. Met. Compd. II* (Eds.: P. Gütllich, H.A. Goodwin), Springer Berlin Heidelberg, Berlin, Heidelberg, **2004**, pp. 23–47.
- [16] S. Hayami, Y. Komatsu, T. Shimizu, H. Kamihata, Y. H. Lee, *Coord. Chem. Rev.* **2011**, *255*, 1981–1990.
- [17] V. A. Grillo, L. R. Gahan, G. R. Hanson, R. Stranger, T. W. Hambley, K. S. Murray, B. Moubaraki, J. D. Cashion, *J. Chem. Soc. Dalton Trans.* **1998**, 2341–2348.
- [18] C. Reus, K. Ruth, S. Tüllmann, M. Bolte, H.-W. Lerner, B. Weber, M. C. Holthausen, M. Wagner, *Eur. J. Inorg. Chem.* **2011**, 1709–1718.
- [19] R. W. Hogue, H. L. C. Feltham, R. G. Miller, S. Brooker, *Inorg. Chem.* **2016**, *55*, 4152–4165.
- [20] A. Arroyave, A. Lennartson, A. Dragulescu-Andrasi, K. S. Pedersen, S. Piligkos, S. A. Stoian, S. M. Greer, C. Pak, O. Hietsoi, H. Phan, S. Hill, C. J. McKenzie, M. Shatruk, *Inorg. Chem.* **2016**, *55*, 5904–5913.
- [21] S. Yergeshbayeva, J. J. Hrudka, J. Lengyel, R. Erkasov, S. A. Stoian, A. Dragulescu-Andrasi, M. Shatruk, *Inorg. Chem.* **2017**, *56*, 11096–11103.
- [22] A. Lennartson, A. D. Bond, S. Piligkos, C. J. McKenzie, *Angew. Chem. Int. Ed.* **2012**, *51*, 11049–11052.
- [23] J. England, R. Gondhia, L. Bigorra-Lopez, A. R. Petersen, A. J. P. White, G. J. P. Britovsek, *Dalton Trans.* **2009**, 5319–5334.
- [24] C. G. Young, *J. Inorg. Biochem.* **2007**, *101*, 1562–1585.
- [25] B. S. Stadelman, M. M. Kimani, C. A. Bayse, C. D. McMillen, J. L. Brumaghim, *Dalton Trans.* **2016**, *45*, 4697–4711.
- [26] M. M. Kimani, H. C. Wang, J. L. Brumaghim, *Dalton Trans.* **2012**, *41*, 5248–5259.
- [27] D. Plaza-Lozano, D. Morales-Martínez, F. J. González, J. Olguin, *Eur. J. Inorg. Chem.* **2020**, 1562–1573.
- [28] H. Toftlund, J. J. McGarvey, in *Spin Crossover Transit. Met. Compd. I* (Eds.: P. Gütllich, H.A. Goodwin), Springer Berlin Heidelberg, Berlin, Heidelberg, **2004**, pp. 151–166.

- [29] O. Prakash, P. Singh, G. Mukherjee, A. K. Singh, *Organometallics* **2012**, *31*, 3379–3388.
- [30] Y.-J. Kim, J. Han, *Bull. Korean Chem. Soc.* **2012**, *33*, 48–54.
- [31] F. Saleem, G. K. Rao, P. Singh, A. K. Singh, *Organometallics* **2013**, *32*, 387–395.
- [32] R. A. A. George B. Kauffman Fred L. Harlan, R. Scott Stephens, Ronald O. Ragsdale, in *Inorg. Synth.* (Ed.: R.W. Parry), **1970**, pp. 251–256.
- [33] J. L. Burmeister, L. E. Williams, *Inorg. Chem.* **1966**, *5*, 1113–1117.
- [34] K. Nakamoto, in *Infrared Raman Spectra Inorg. Coord. Compd. Part B* (Ed.: Wiley-Interscience), **2008**, pp. 1–273.
- [35] A. H. Norbury, in *Adv. Inorg. Chem. Radiochem.* (Eds.: H.J. Emeléus, A.G. Sharpe), Academic Press, **1975**, pp. 231–386.
- [36] S. Rodríguez-Jiménez, S. Brooker, *Inorg. Chem.* **2017**, *56*, 13697–13708.
- [37] A. Spek, *Acta Crystallogr. Sect. C* **2015**, *71*, 9–18.
- [38] F. Anthony Deeney, C. J. Harding, G. G. Morgan, V. McKee, J. Nelson, S. J. Teat, W. Clegg, *J. Chem. Soc. Dalton Trans.* **1998**, 1837–1844.
- [39] M. G. B. Drew, C. J. Harding, V. McKee, G. G. Morgan, J. Nelson, *J. Chem. Soc. Chem. Commun.* **1995**, 1035–1038.
- [40] M. A. Halcrow, in *Spin-Crossover Mater.* (Ed.: M.A. Halcrow), **2013**.
- [41] G. Novitchi, S. Jiang, S. Shova, F. Rida, I. Hlavička, M. Orlita, W. Wernsdorfer, R. Hamze, C. Martins, N. Suaud, N. Guihéry, A.-L. Barra, C. Train, *Inorg. Chem.* **2017**, *56*, 14809–14822.
- [42] G. Carver, P. L. W. Tregenna-Piggott, A.-L. Barra, A. Neels, J. A. Stride, *Inorg. Chem.* **2003**, *42*, 5771–5777.
- [43] A. Ozarowski, S. A. Zvyagin, W. M. Reiff, J. Telser, L.-C. Brunel, J. Krzystek, *J. Am. Chem. Soc.* **2004**, *126*, 6574–6575.
- [44] T. Sugaya, T. Fujihara, T. Naka, T. Furubayashi, A. Matsushita, H. Isago, A. Nagasawa, *Chem. – Eur. J.* **2018**, *24*, 17955–17963.
- [45] The calculation of the remaining HS-state percentage at low temperature for complex **1b** was performed using the χ_{MT} parameter, instead of the μ_{eff} value, due to the linear relationship of χ_{MT} of the spin state mixture: $\chi_{MT}(\text{mixture}) = \gamma_{\text{HS}}(\chi_{MT})_{\text{HS}} + \gamma_{\text{LS}}(\chi_{MT})_{\text{LS}}$, γ = mole fraction.
- [46] R. Kulmaczewski, J. Olguin, J. A. Kitchen, H. L. C. Feltham, G. N. L. Jameson, J. L. Tallon, S. Brooker, *J. Am. Chem. Soc.* **2014**, *136*, 878–881.
- [47] S. Brooker, *Chem. Soc. Rev.* **2015**, *44*, 2880–2892.
- [48] A. J. Fitzpatrick, E. Trzop, H. Muller-Bunz, M. M. Dirtu, Y. Garcia, E. Collet, G. G. Morgan, *Chem Commun* **2015**, *51*, 17540–17543.
- [49] H. Beraldo, L. Tosi, *Inorganica Chim. Acta* **1983**, *75*, 249–257.
- [50] D. Sellmann, J. Utz, N. Blum, F. W. Heinemann, *Coord. Chem. Rev.* **1999**, *190–192*, 607–627.
- [51] M. A. Halcrow, *Chem. Lett.* **2014**, *43*, 1178–1188.
- [52] S. Vela, H. Paulsen, *Inorg. Chem.* **2018**, *57*, 9478–9488.
- [53] P. Gütlich, Y. Garcia, H. Spiering, in *Magn. Mol. Mater. IV* (Eds.: J.S. Miller, M. Drillon), John Wiley & Sons, Ltd, **2003**, pp. 271–344.
- [54] G. Sheldrick, *Acta Crystallogr. Sect. A* **2008**, *A64*, 112–122.
- [55] P. Remuzon, D. Bouzard, P. DiCesare, M. Essiz, J.-P. Jacquet, A. Nicolau, A. Martel, M. Menard, C. Bachand, *Tetrahedron* **1995**, *51*, 9657–9670.

Entry for the Table of Contents



The effect of the chelate ring and NCE co-ligand on the magnetic behaviour in complexes of the type $[\text{Fe}^{\text{II}}(\text{N}_2\text{S}_2)(\text{NCE})_2]$ based on picolythioether ligands is shown. A structural analysis has been performed, confirming that the Fe-N-C(E) angle is a good marker that could permit predicting SCO-behaviour, and in addition, we have shown that the N-C(E) bond length is useful too as a predicting marker.

Institute and/or researcher Twitter usernames: @Leolguin (Dr. J. Olguín)